Reproductive isolation due to divergent ecological selection is accompanied by vast genomic instability in experimentally evolved yeast populations

Running head: Ecological isolation barriers in yeast

*Devin P. Bendixsen[1,2], Ciaran Gilchrist[1], Chloé Haberkorn[1], Karl Persson[3], Cecilia Geijer[3], Jonas Warringer[4], Rike Stelkens[1]**

[1] Department of Zoology, Stockholm University, Svante Arrheniusväg 18 B, 106 91 Stockholm, Sweden

[2] Department of Genetics, Harvard Medical School, 77 Avenue Louis Pasteur, 02115, Boston, MA, USA

[3] Division of Industrial Biotechnology, Department of Life Sciences, Chalmers University of Technology, Kemigården 1, 412 96 Göteborg, Sweden

[4] Department of Chemistry and Molecular Biology, University of Gothenburg, Medicinaregatan 9C, 41390 Göteborg, Sweden

* Corresponding author: Rike Stelkens, Department of Zoology Stockholm University, telephone: +46 (0) 816 4223; email: rike.stelkens@zoologi.su.se

Devin Bendixsen: 0000-0003-0831-7646; devin.bendixsen@gmail.com

Ciaran Gilchrist: 0000-0002-7639-6131; ciaran.gilchrist@umu.se

Chloé Haberkorn: 0000-0002-7371-9177; chloe.haberkorn@zoologi.su.se

Karl Persson: 0000-0002-2173-8165; karperss@chalmers.se

Cecilia Geijer: 0000-0002-4158-2938; cecilia.geijer@chalmers.se

Jonas Warringer: 0000-0001-6144-2740; jonas.warringer@cmb.gu.se

Rike Stelkens: 0000-0002-8530-0656; rike.stelkens@zoologi.su.se

Abstract

Populations evolving independently in divergent environments accumulate genetic differences and potentially evolve reproductive isolation as a by-product of divergence. The speed and mechanisms underlying this process are difficult to investigate because we rarely get the opportunity to witness them in natural settings, and histories of selection and gene flow between populations are often unknown. Here, we experimentally evolved yeast for 1000 generations of evolution in both divergent and parallel environments. At regular time points during experimental evolution, we made crosses between parallel- and divergent-evolving populations to measure postzygotic reproductive isolation (gamete viability). We used whole genome population sequencing to determine the mutational load, the number and types of structural variation, and other genomic features of the parent, F1, and F2 intraspecific hybrids. We found evidence for large scale phenotypic and genome-wide differentiation in response to divergent laboratory selection. Divergent-selected populations produced hybrids with reduced gamete viability - a classic signature of postzygotic reproductive isolation in the form of hybrid breakdown. Parallel-selected populations on the other hand remained more reproductively compatible (with exceptions). We found that F2 hybrid genomes contained vast genomic instability, i.e., new structural variants (especially insertions, deletions, and interchromosomal translocations) that were not observed in parent and F1 genomes, which is likely a result of chromosome missegregation and recombination errors in hybrid meiosis. Our results provide phenotypic and genomic evidence that partial reproductive isolation evolved due to adaptation to divergent environments, consistent with predictions of ecological speciation theory.

Keywords: experimental evolution, hybridization, mutational load, reproductive isolation, *Saccharomyces,* structural variation

Introduction

Ecological speciation implies a process by which adaptation to different ecological niches, in allopatry or sympatry, leads to the evolution of reproductive isolation between populations (Mayr 1947; Rice and Hostert 1993; Schluter 2001; McKinnon et al. 2004; Nosil 2012). Long-term monitoring of natural populations has been valuable in linking ecological traits with the emergence of reproductive barriers (e.g. (Filchak et al. 2000; Rundle et al. 2000; Grant and Grant 2003; Funk et al. 2006; Sawada et al. 2022)), providing convincing arguments for ecological factors to play a role in driving population divergence. However, ecological speciation remains difficult to demonstrate because it usually proceeds over extended evolutionary times (Hendry et al. 2007), trait divergence is often cryptic (Struck et al. 2018; Sparks et al. 2022), and the evolutionary histories of natural populations are challenging to reconstruct. It is usually unknown whether divergent selection was present, how long it lasted, and what the timing and amount of gene flow was between populations. Thus, it often remains unclear, especially between allopatric species pairs occupying different niches, whether divergent, ecology-based selection was the driving force underlying their divergence, eventually leading to speciation (Anderson and Weir 2022; Irestedt et al.; Müller et al.). Due to these constraints, studies have often relied on combinatorial approaches, using i) data on niche divergence in traits related to habitat use, such as resource utilization or foraging behavior (e.g. (Hatfield and Schluter 1999; Nosil and Crespi 2006; Munar-Delgado et al. 2024), ii) data on reproductive barriers, such as differences in mating behaviors or flowering times reducing gene flow between populations adapted to different ecological niches (e.g. (Dieckmann et al. 2004; Villa et al. 2019)), and iii) genetic data, detecting signatures of selection and divergence in genetic regions associated with ecological adaptation and reproductive isolation (e.g. (Nosil and Schluter 2011; Härer et al. 2021; Louder et al. 2024)).

Microbial experimental evolution provides a powerful tool for investigating questions in evolutionary biology. It has been used to describe the dynamics and genetic mechanisms underlying

72 adaptation to stable (Lenski et al. 1991; Good et al. 2017; Johnson and Desai 2022), heterogenous
73 (Rainey and Travisano 1998), or changing environments (Bell and Gonzalez 2011; Gorter et al. 2016;
74 Gorter et al. 2017) and to test theoretical predictions about adaptation rates in sexual versus asexual
75 populations (McDonald et al. 2016; Kosheleva and Desai 2018; Leu et al. 2020). Experimental evolution
76 with microbes can also provide insights on fundamental questions in speciation, especially about the
77 early stages of divergence, i.e. why, how and when lineages split (Stelkens 2024). Microbial genomes are
78 often small and generation times are short, allowing for evolve-and-resequencing approaches to capture
79 speciation and its underlying genetic basis in action. For instance, experimental evolution with a virus
80 (lambda bacteriophage) and its bacterial host (*Escherichia coli*) has demonstrated that divergent
81 ecological selection caused the phages to split into two genetically distinct lineages with different host
82 preferences, and that barriers to gene flow formed as a consequence of ecological specialization, which
83 resulted in reproductive isolation (Meyer et al. 2016). Experiments with yeast and other fungi have
84 shown that divergent selection can lead to phenotypic divergence and rapid ecological differentiation
85 (Dettman et al. 2007; Dettman et al. 2008; Ament-Velásquez et al. 2022), even under high rates of gene
86 flow (Tusso et al. 2021). But generally, there is a lack of studies that combine both organismal and
87 genetic approaches to measure reproductive isolation (Westram et al. 2022). Work investigating the
88 emergence and dynamics of reproductive isolation using repeated measures of hybrid viability across
89 generational time scales, from the beginning to later stages of parental divergence under controlled
90 environmental conditions, could significantly advance our understanding of what can drive the evolution
91 of reproductive isolation in the early stages of speciation.

92 Here, we used experimental evolution with the budding yeast *Saccharomyces cerevisiae* and
93 propagated replicate, asexually reproducing populations in both different and parallel (same)
94 environments for 1000 mitotic generations (**Figure 1**). At regular time points of population divergence,
95 we generated sexual F1 and F2 (hybrid) crosses between and within environments, to test whether

96 reproductive isolation evolved and increased with time. We evolved populations in four distinct
97 selective environments and profiled parental phenotypes in 90 different environments to test for
98 phenotypic divergence over time. We then used whole genome sequencing on parental, F1, and F2
99 hybrid populations to measure their mutational load and other measures of genomic stability. By the
100 endpoint of experimental evolution, we found that divergent-selected populations were up to 50%
101 reproductively isolated due reduced hybrid gamete viability, while most crosses made between parallel-
102 selected populations remained genetically compatible. We detected vast structural variation in the F2
103 hybrid genomes, including up to three times more deletions, insertions, inversions, tandem duplications,
104 and interchromosomal translocations than in the diploid parental and F1 hybrid genomes. Consistent
105 with predictions of ecological speciation theory, our results suggest that divergent adaptation has led to
106 partial reproductive isolation, accompanied by severe genomic instability in the hybrids. This instability
107 may be the result of structural genetic differences accumulating in parental populations causing
108 recombination errors and chromosome missegregation during hybrid meiosis, but further work is
109 needed to test if this genetic mechanism underlies the evolution of reproductive isolation in our system.
110

111 **Materials and Methods**

112 ***Founder populations***

113 We generated large diploid, and genetically diverse, founder populations of yeast through mating and
114 mass sporulation of two related *S. cerevisiae* strains (SK1 and Y55; Figure 1) as previously described
115 (Ament-Velásquez et al. 2022), for which high quality reference genomes are available (Peter et al. 2018;
116 Bendixsen, Gettle, et al. 2021). Briefly, SK1 and Y55 were genetically modified to introduce
117 auxotrophies, which were used as selective markers to exclude non-mated haploids (non-hybrids). From
118 these strains, two founding populations were generated that only differed in the selective markers they
119 carried. These selective markers allowed us to mass-mate the NaCl-evolved populations with

120 populations evolving in the other three environments, while safely removing all non-hybrid parental
121 genotypes, using a selective growth medium. In the synthetic complete growth medium we used for
122 experimental evolution, these auxotrophic markers have no detectable fitness effect as all essential
123 amino acids are provided. The founders of populations evolving in NaCl (called "N founder" below) are
124 the diploid recombined offspring of a cross between SK1 (MATα ho:KanMX ura3::ClonNat) and Y55
125 (MATa ho leu2::HygMX ura3::ClonNat). Founders of the populations evolving in ethanol and two
126 different concentrations of lithium acetate (called "LE founder" below), are the diploid recombined
127 offspring of a cross between SK1 (MATα ho:KanMX lys2::ClonNat) and Y55 (MATa ho leu2::HygMX
128 lys2::ClonNat). Despite having different selective markers, it is important to note that both founders
129 maintain the same strain background and differ only in their fitness-neutral auxotrophic markers.
130
131 ***Experimental evolution of parental populations***
132 From these founders, replicate populations (from here on 'parental´ populations) were experimentally
133 evolved in four divergent environments, each with four replicates (considered parallel-evolved) for up to
134 1000 asexual generations (**Figure 1**). The number of generations was estimated by counting cells after
135 48h growth in selective media in the highest stress environment (0.75M NaCl, see Ament-Velásquez et
136 al. 2022). This approach is conservative because it likely underestimates the number of generations in
137 the other, less stressful environments. All evolution environments contained synthetic complete (SC)
138 medium (2% glucose, 0.67% bacto-yeast nitrogen base without amino acids, 0.00079% Formedium CSM
139 powder (product code DCS0019), made up to 1L with sterilised deionised water) plus one of the
140 following substances to induce stress: 0.75M sodium chloride (from here on NaCl), 8% ethanol (C_2H_6O,
141 from here on EtOH), and two different concentrations of lithium acetate ($C_2H_3LiO_2$, from here on
142 LiAc0.01M and LiAc0.02M). The correct volume of EtOH was added to the test tube just before
143 inoculation to limit evaporation. We have previously demonstrated that these four media significantly

differ in how much they reduce the fitness of populations, and we have provided phenotypic and genetic evidence that populations become differentially adapted to these environments (Ament-Velásquez et al. 2022).

Three to four replicate populations were evolved in separate test tubes containing 5mL of SC media with one of the four substances. Then, we serially transferred 10µL of yeast culture every 48 hours to fresh media (approximately seven generations, estimated by counting cells after 48 hours). Every five transfers (10 days, i.e. ~35 generations), a 900µL sample of each population was frozen in 44% glycerol at -70°C for later use. The experiment was run for a total of ~300 days. After some cross-replicate contamination was detected using sequencing data (Ament-Velásquez et al. 2022), we excluded two NaCl-evolved replicate populations (R1 and R4) at 1000 generations, all LiAc0.01M and LiAc0.02M-evolved populations at 1000 generations, and one LiAc0.01M-evolved population (R3) at all generations. No crosses were generated from these contaminated populations. Retained populations showed no signs of cross-contamination in terms of shared single nucleotide variants.

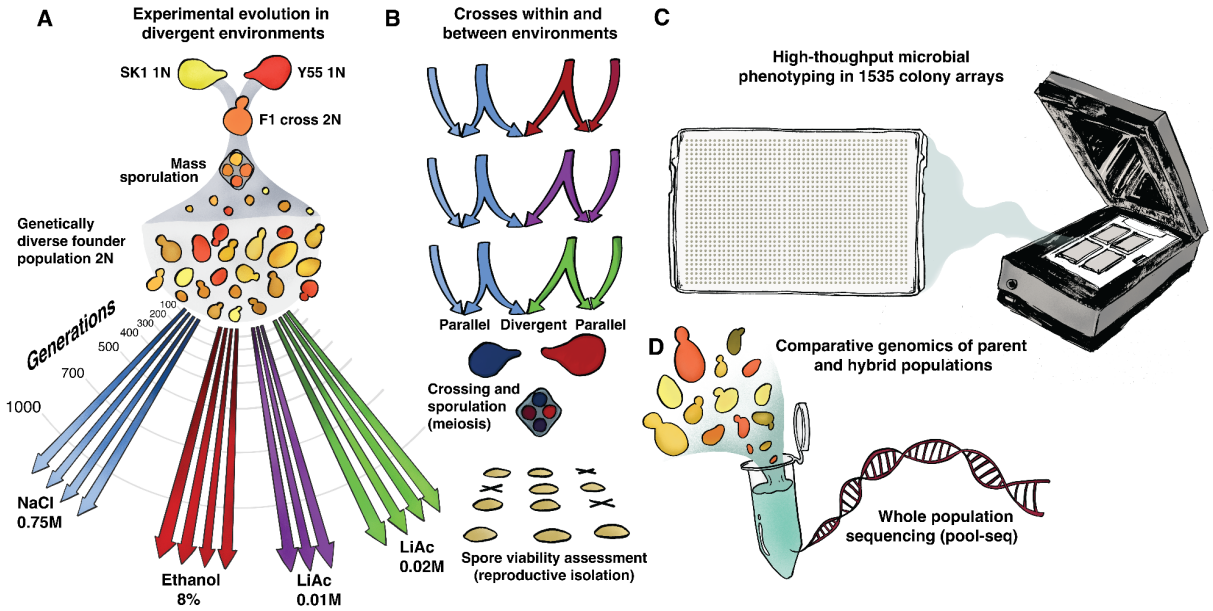

Figure 1: Overview of experimental approaches. A) Experimental Evolution: A founder population was generated by the mating of two *S. cerevisiae* strains (SK1 and Y55), followed by mass sporulation (meiosis). This genetically diverse, diploid founder was split into four different environments, containing growth medium with either 0.75M NaCl, 8% EtOH, 0.01M lithium acetate, or 0.02M lithium acetate, and

evolved for up to 1000 asexual generations by serial transfer, in three or four independent biological replicates per environment (Ament-Velásquez et al. 2022). 2N indicates diploid, 1N indicates haploid genotypes. **B) Crossing design**: At seven points of parental divergence (indicated by the curved grey lines in A), sexual hybrid crosses were made between NaCl-populations and populations from all other environments (with replication). Control crosses were made between parallel-evolved, replicate populations from the same environment. Crosses from five time points were then sporulated and the viability of the haploid F2 offspring was assessed after tetrad dissection. **C) High throughput phenotyping:** To assess phenotypic divergence, the growth of parental populations sampled from five time points of experimental evolution was measured in 90 non-selection environments using colony image scans. **D) Comparative genomics** using pool sequencing of parental, F1, and F2 populations sampled at seven time points of experimental evolution.

Hybridization at increasing timepoints of parental divergence

We generated hybrid crosses at 100, 300, 500, 700, and 1000 generations of parental divergence, between all four replicate NaCl-populations (excluding R1 and R4 at 1000 generations due to contamination) and up to four replicate populations from each of the three other environments (LiAc 0.01M (3 replicates), LiAc 0.02M (4 replicates) and EtOH (4 replicates); **Figure 1**). Due to the selectable markers present in the parents, NaCl- populations could be mass-crossed with the other three populations while safely removing all non-hybrid parental genotypes using a selective medium (described below). First, we mass-sporulated the diploid parental populations. For this, 500µL of saturated culture were added to 50mL of sporulation medium (1% potassium acetate, 0.05% glucose, 0.1% yeast extract, and H_2O to 1L) and left for 5 days with gentle shaking at room temperature. We then mixed 500µL of each of the two parent spore cultures together in a 1.5mL Eppendorf tube, and centrifuged the culture down to a pellet to induce mating. To select for F1 hybrids, we inoculated 25µL of the pellet in 5mL of -lys SD medium with G418 (0.67% bacto-yeast nitrogen base without amino acids, 2% glucose, dropout powder (-lys), G418 400mgL^{-1} and H_2O to 1L). This selects for F1 hybrid genotypes in bulk, which are heterozygous for both selective markers (-lys and G418). Note that this mass mating and sporulation protocol permitted F1 hybrid populations to contain genetic diversity, depending on how many different parental genotypes participated in the mass mating. To generate F2 hybrid

192 populations, we put F1 hybrid populations through one round of meiosis by mass sporulating them in
193 50mL of sporulation medium for 5 days with gentle shaking at room temperature. F1 AND F2 hybrid
194 populations were stored at -70°C in 22% glycerol solution for whole genome sequencing.
195
196 ***Assessing parental phenotypic divergence***
197 We phenotypically profiled all parent populations (i.e. populations evolved in NaCl, LiAc 0.01M, LiAc
198 0.02M, and EtOH) in 90 different environments, at five time points of divergence (at 100, 300, 500, 700,
199 and 1000 generations), using the Scan-o-Matic system for high-throughput microbial phenotyping
200 (Zackrisson et al. 2016; Li et al. 2019; Alalam et al. 2020; Mukherjee et al. 2021; Persson et al. 2022;
201 Stenberg et al. 2022) version 2.2 (https://github.com/Scan-o-Matic/scanomatic.git). Parental
202 populations were precultured in SC media for 48h in 96-well plates at 30°C without shaking and frozen.
203 Then, cultures were pinned directly from thawed cryo-stocks in 96-format for preculturing on agar
204 plates (for more detailed methods see (Persson et al. 2024)). Samples were split into duplicates (two 96-
205 well plates). A third plate was used for propagation of a spatial control, containing a Y55 diploid strain.
206 After preculture, populations were pinned onto 1536 colony arrays on agar plates robotically (Singer
207 ROTOR HDA), allowing for accurate measuring of colony growth using the Scan-o-matic software. The
208 spatial control was placed in every fourth position (in total 384 colonies per plate) to remove any spatial
209 bias, irregularities in the plates, or other bias from the local area. In total, 52 distinct stressors were used
210 in different concentrations, resulting in 90 distinct environments, including superoxidative stress (e.g.
211 paraquat), heavy metals (e.g. $CuSO_4$), different carbon sources (e.g. maltose), antifungal drugs (e.g.
212 Clotrimazole). Phenotypic data, i.e. growth measurements, are reported in Table S1, with the full list of
213 environments in Table S2. Cultivation plates were maintained undisturbed and without lids for the
214 entire duration of the assay (72h) in high-resolution desktop scanners (Epson Perfection V800 PHOTO
215 scanners, Epson Corporation, UK) at 30°C, in moisture-controlled thermostatic cabinets with air

216 circulation. We imaged plates at 20-minute intervals using transmissive scanning at 600 dpi and
217 extracted intensities for pixels included in, and outside, each colony. We estimated the sum pixel
218 intensity for each colony, subtracted the median pixel intensity of the local background, and
219 transformed the remaining cell-associated pixel intensity to cell counts by using a pre-established
220 calibration function, established using both spectrometry and flow cytometry (Zackrisson et al. 2016).
221 We smoothed and quality-controlled growth curves, rejecting approximately 0.3% of growth curves as
222 erroneous, blind with respect to sample identities. Based on the number of cells after 72h, we used the
223 yield normalized against the spatial control (Y55 diploid).
224 A custom 'ParentalDivergence' function was generated in R, using normalized yield, the number
225 of generations in experimental evolution, and the type of population comparison. Mean and double
226 standard deviations of normalized yields were first computed for each of the 90 environments for each
227 of the replicate parent 1 (P1) and 2 (P2) populations. This was done for each type of population
228 comparison, i.e. divergent-environment comparisons (NaCl x EtOH, NaCl x LiAc0.01, NaCl x LiAc0.02) and
229 parallel-environment comparisons (NaCl x NaCl, EtOH x EtOH, LiAc0.01 x LiAc0.01, LiAc0.02 x LiAc0.02).
230 We considered fitness to be higher if the normalized mean yield of P2 was larger than the normalized
231 mean yield of P1 plus P1's double standard deviation (i.e. mean P2 > mean P1 + 2σ). We considered
232 fitness to be lower if the normalized mean yield of P2 was lower than the normalized mean yield of P1
233 minus P1's double standard deviation, following previous protocols (i.e. mean P2 < mean P1 - 2σ; see
234 (deVicente and Tanksley 1993; Brice et al. 2021). Parental phenotypic divergence is thus defined as the
235 proportion of the 90 environments in which there was a large difference in yield between the two
236 populations compared.
237

238 ***Assessing reproductive isolation***

239 To measure productive isolation between the parental yeast populations evolving in divergent and
240 parallel environments, we mated together individual parent genotypes to produce F1 crosses, after 100,
241 300, 500, 700 and 1000 generations of experimental evolution. F1 were then sporulated to produce F1
242 spores (gametes), which are their recombined, haploid F2 offspring, and reproductive isolation was
243 measured as the fraction of unviable F2 gametes. For this, F1 crosses were plated onto solid YPD agar
244 medium (1% yeast extract, 2% peptone, 2% glucose, 2% agar made up to 1L with sterilized deionized
245 H_2O) and grown for 2 days, followed by replica plating onto solid KAc medium (1% potassium acetate,
246 0.05% glucose, 0.1% yeast extract and H_2O to 1L) for sporulation. Populations were left for 2-7 days,
247 until tetrads were identified under the microscope. Yeast tetrads usually contain four spores (gametes),
248 which are the recombined haploid products of meiosis. Sporulated cultures with tetrads were incubated
249 for one hour at room temperature in 10µL of filter sterilized zymolyase solution (1mg of zymolyase per
250 1mL of 1M sorbitol solution) to kill vegetative (unsporulated) cells and digest the outer membrane of the
251 tetrads, surrounding the ascospores. Cell lysis was terminated by adding 500µL of sterilized H_2O. To
252 assess the fertility of F1 hybrid crosses, we dissected 10-20 individual F1 tetrads, and measured the
253 survival rates of their haploid F2 offspring. Tetrads were dissected on YPD plates using a Singer MSM
254 400 robot. Individual spores were then left to germinate and grow for 72h at 30°C, at which point spore
255 viability was assessed. Spores were counted as viable based on the presence of colonies visible to the
256 eye. Thus, gamete viability was assessed as the capacity to germinate and show sufficient growth to
257 form macroscopic colonies, which is a standard method in yeast genetics. The total proportion of
258 unviable spores per cross was calculated from 20 dissected tetrads (80 spores) at 100, 700, and 1000
259 generations, and 10 tetrads (40 spores) at 300 and 500 generations of parental divergence.

260 To assess the F1 fertility of the control crosses, i.e. crosses between replicate parental
261 populations that evolved in parallel environments, we used the same mating, sporulation and dissection

262 protocols as described above. The total proportion of unviable spores (gametes) per cross was
263 calculated from 10 dissected tetrads (40 spores) at 100, 500, 700 and 1000 generations of parental
264 divergence.
265
266 ***DNA extraction and whole-genome sequencing***
267 DNA was extracted as described in (Ament-Velásquez et al. 2022). We extracted DNA from whole
268 parental, F1, and F2 hybrid populations, respectively, at seven time points each (0, 100, 200, 300, 400,
269 500, 700, and 1000 generations). Extraction was carried out on overnight culture, with ~1mL of culture
270 used. Library preparation and sequencing were performed at the Science for Life Laboratories
271 (Stockholm, Sweden), using the Illumina Nextera Flex protocol. Sequencing was done using either
272 NovaSeq S4-300 (2x150bp) or NovaSeq S-Prime (2x150bp) to an estimated median depth of coverage
273 per sample of around 30x to 780x. The raw sequences were deposited in the European Nucleotide
274 Archive, parental populations are available at accession number PRJEB46680, while hybrids are available
275 at accession number PRJEB83568.
276
277 ***Sequencing read quality and genome alignment***
278 FastQC v.0.11.9 (Andrews 2010) was used to assess the quality of raw sequencing reads and reads were
279 trimmed using Trimmomatic v0.36 (Bolger et al. 2014). Sequencing reads were aligned to a S288C
280 reference genome (R64; GenBank accession GCA_000146045.2) using BWA mem v0.7.17-r1188 (Li and
281 Durbin 2009) and SAMtools v1.11 (Danecek et al. 2021) was used to sort and index the resulting
282 mapping file. Duplicated reads were flagged and removed using Picard v3.1.0
283 (http://broadinstitute.github.io/picard/), followed by quality assessment using Qualimap v2.3
284 (Okonechnikov et al. 2016).
285

286 ***Assessing the genomic mutational landscape***

287 To assess the mutational landscape of each experimentally evolved, parental yeast population and the
288 F1 and F2 crosses made between them, we measured the amount of variants detected across
289 mutational scales, ranging from single nucleotide variants to entire chromosome aneuploidies. To
290 identify small mutational variants (SNV and indels), we used freebayes v1.3.6 (Garrison and Marth 2012)
291 with default parameters. Identified variants were filtered using VCFtools v0.1.16 (Danecek et al. 2011) to
292 include only variants with minimum quality (minQ) >30 and sequencing read depth (minDP) >5. SnpEff
293 v5.2 (Cingolani et al. 2012) was used to assess and annotate the effect of identified mutational variants
294 on genes using the database of the reference genome R64-1-1.105 with canonical transcripts. To
295 identify structural variants including insertions, deletions, inversions, tandem duplications and
296 interchromosomal translocations we used Manta v1.6.0 (Chen et al. 2016) with default parameters.
297 Structural variant detection is limited by the read pair fragment size. To more comprehensively assess
298 the genome-wide copy number variation (amplifications and deletions), we used Control-FREEC v11.6
299 (Boeva et al. 2011; Boeva et al. 2012) with baseline ploidy = 2, a break-point threshold = 0.8 and
300 coefficient of variation = 0.5 (Scopel et al. 2021). We further optimized the CNV detection by limiting the
301 expected GC content to between 0.35 and 0.55. Variants were further filtered to only include copy
302 number calls that were statistically significant ($p<0.05$) using Wilcoxon Rank Sum Test and a Kolmogorov
303 Smirnov Test. Two metrics of CNVs were assessed for differences across time and between populations:
304 CNV load and the fraction of the genome altered. CNV mutational load is the number of CNV events
305 (amplification or deletion) detected within a population. The fraction of genome altered incorporates
306 the size of each CNV event to determine the amount of the genome that is altered by CNVs. We also
307 differentiated between small (<10kb) and large (>10kb) CNVs. Chromosomes were further considered
308 aneuploid if >60% of the chromosome was identified as amplified or lost. To better assess the
309 differences that might have existed between the two founding populations and potentially their lasting

310 effects through time, we re-analyzed sequencing data from the original study (Ament-Velasquez et al.
311 2022), which was focused on the genetic basis of evolutionary adaptation of these founders. This study
312 included sequencing data collected at shorter time-points, in particular within the first 100 generations
313 (30 and 60 generations). We analyzed the relative sequencing read depth to determine how persistent
314 the aneuploidies identified in the founding populations (generation 0) were during adaptation.
315
316 ***Calculating population differentiation (F_{st}) and genome similarity (Jaccard index)***
317 We calculated pairwise F_{st} between all divergent- and parallel-evolving parental populations at each of
318 the sampled timepoints, based on single nucleotide polymorphisms (SNPs). We first combined the vcf
319 files generated from freebayes using bcftools v1.19 (Danecek et al. 2011), with parallelization of file
320 compression by gnuparallel v20230422 (Tange 2011), using the default parameters of bcftools merge
321 and the R package poolfstats v2.2.0 (Gautier et al. 2022) on R v3.4 (R Core Team 2023). First the vcf files
322 were converted to pooldata objects, using vcf2pooldata with the default parameters. F_{st} was then
323 calculated using pairwiseFST with the nsnp.per.bjack.block = 150 to calculate the Block-Jackknife
324 estimation of standard error, using an ANOVA framework (Hivert et al. 2018). Similarities between copy
325 number variation calls in different populations and through time were assessed based on the Jaccard
326 similarity coefficient using CNVmetrics R package v3.20 (Belleau et al. 2021; Deschênes et al. 2022).
327
328 **Results**
329 We experimentally evolved yeast populations for 1000 generations in divergent and parallel
330 environments. The four selection environments contained either salt, ethanol, or two different
331 concentrations of lithium acetate, and significantly differed in the degree to which they reduced the
332 fitness of the founder populations. We have previously provided phenotypic and genetic evidence that
333 these populations become differentially adapted to these environments (Ament-Velásquez et al. 2022).

334 At five time points during experimental evolution, we made crosses between the parallel- and divergent-
335 evolving populations (the 'parents') to measure postzygotic reproductive isolation (F1 spore viability). At
336 seven time points, we used whole population genome sequencing on parents, F1, and F2 hybrids, to assess
337 their mutational load, i.e. the number and types of structural variation, and other genomic features.
338
339 ***Parental phenotypic divergence***
340 We phenotypically profiled the evolving parent populations in 90 non-selection environments. These
341 environments contained the same medium (SC) as the selective environments used for experimental
342 evolution, but they also each contained an additional growth limiting substance (Table S2). Thus, our
343 measure of phenotypic divergence between populations is likely a conservative estimate. Note that we
344 only assessed the phenotypic divergence of evolving parent populations here (not the F1 or F2 crosses),
345 to test for adaptation as a result of divergent ecological selection in the parents.
346 As expected, with increasing generations of experiment evolution in different environments,
347 divergent-selected parent populations significantly diverged in phenotype (regression across all
348 divergent-evolved populations: R = 0.14, p = 0.007; when removing the outliers at G1000: R = 0.09, p =
349 0.036; **Figure 2A**). Regression of individual environment comparisons resulted in significantly increasing
350 phenotypic divergence in the NaCl vs. EtOH-evolved populations (R = 0.41, p=0.004), but not for the
351 other two comparisons.
352 In contrast, parent populations evolving in parallel in the same environment did not diverge
353 phenotypically (R = 9.34e-04, p = 0.81; when removing the outliers at G1000: R = 0.002, p = 0.768; **Figure**
354 **2B**). Here, individual regression of the EtOH vs. EtOH-evolved populations resulted in a significant
355 decrease of phenotypic divergence with generations (R = 0.51, p = 0.006) but this trend was no longer
356 significant when removing the outlier at G1000 (R = 0.30, p = 0.066). This suggests that the phenotypic

357 divergence of populations evolving under different selection pressures was caused by ecological

358 differences between the four selection environments.

359

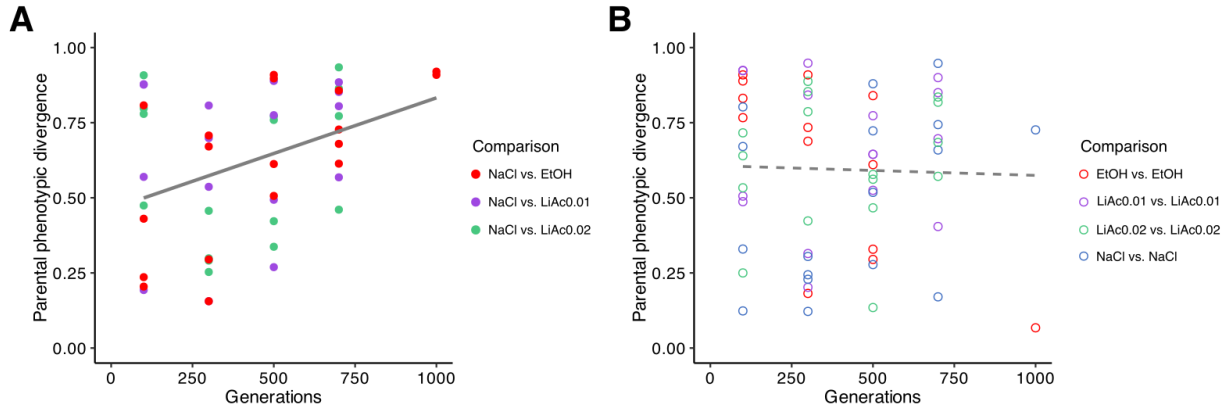

360
361 **Figure 2**: **Phenotypic divergence of evolving parental populations.** Parental phenotypic divergence (the
362 proportion of 90 environments, in which populations significantly differed in yield) at five time points
363 (number of generations) of experimental evolution. **A)** Comparisons between divergent-evolved
364 populations in different environments. **B)** Comparisons between parallel-evolved populations in the
365 same environment. Solid line indicates significant regression, dashed line shows non-significant
366 regression across all comparisons.
367

368 ***Genetic population differentiation***

369 When comparing parental populations, genetic population differentiation (genome-wide F_{st}) was

370 generally larger (mean = 0.25) in pairwise comparisons between divergent-selected (grey boxes in **Figure**

371 **3A**) than between parallel-selected populations (mean = 0.19, colored boxes). The only exception were

372 comparisons between parallel-selected LiAc0.01 populations (purple), which produced slightly higher F_{st}-

373 values but were not significantly larger than the divergent-selected populations. F_{st} -values increased

374 with the number of generations of evolution in both divergent and parallel environments (**Figure 3A**,

375 Figure S1), except for comparisons between divergent-selected NaCl and LiAc0.02 populations. NaCl and

376 LiAc0.02 populations tended to decrease in F_{st} over time. This may be the result of populations losing

377 genetic variation overall, which was particularly the case for LiAc0.02 populations as discussed below.

378 Importantly, the two founding populations with compatible selective markers were found to have a very

379 low pairwise F_{st}-value suggesting a high level of genetic similarity and low amount of differentiation

380 (Figure S2).

381 Consistent with their lower F_{st} -values overall, the genomes of parallel-selected populations

382 remained significantly more similar (using the Jaccard similarity index) than the genomes of divergent-

383 selected populations (gray boxes in **Figure 3B**). Together, this suggests that the larger genetic divergence

384 of populations evolving under different selection pressures was caused by ecological differences

385 between the four selection environments.

386

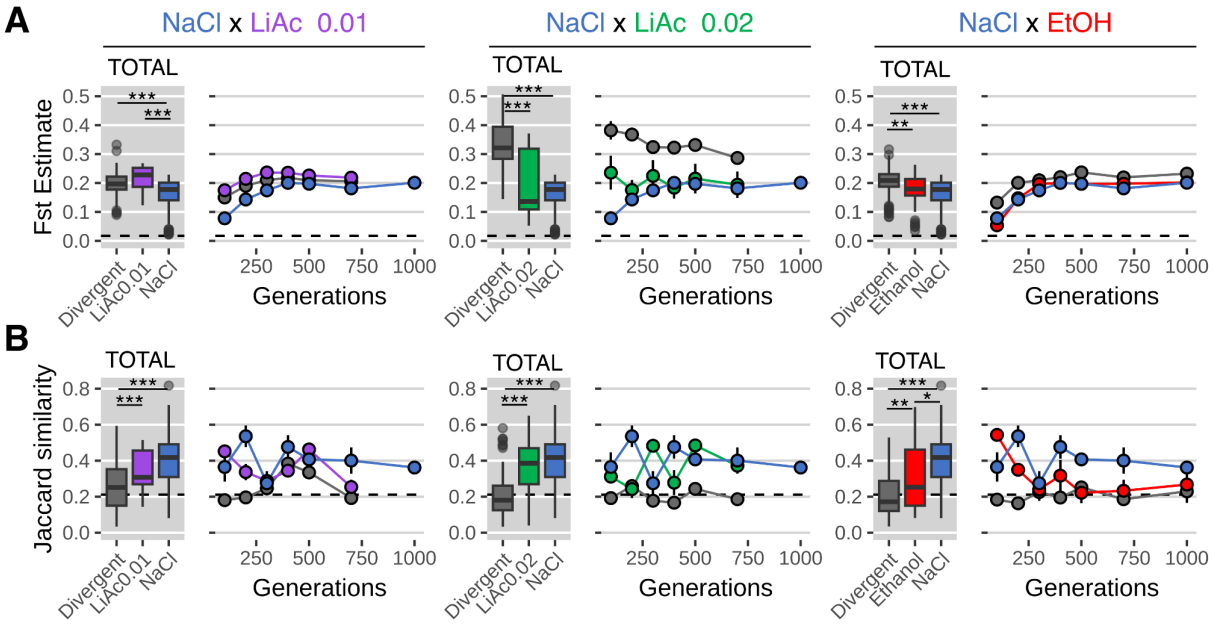

387

388 **Figure 3: Parental genomic population differentiation**. **A)** Genetic population divergence (F_{st}) at seven
389 time points (n of generations) of experimental evolution. . Boxplots indicate the first and third quartiles
390 with whiskers extending to the furthest point not exceeding 1.5 x the interquartile range and outliers
391 beyond this are shown as dots. The solid line indicates the median value. **B)** Genomic similarity (Jaccard
392 similarity index) at seven time points (n of generations) of experimental evolution. Box plots show
393 means (thick horizontal line) across all generations of each population type. Circles indicate the mean
394 measurement and the vertical line indicates the standard error of the mean. 'Divergent' indicates
395 comparisons between divergent-selected populations. Asterisks indicate statistical significance using
396 Kruskal-Wallis and pairwise Wilcoxon post hoc tests with Bonferroni corrections (adjusted p-values <
397 0.001 = ***, < 0.01 = **, < 0.05 = *). Dashed horizontal lines indicate the measured differentiation
398 between the founder populations at the beginning of evolution.

399

400 ***F2 hybrid viability***

401 The viability of F1 spores made between divergent-selected populations was significantly lower than the
402 viability of crosses made between parallel-selected populations on average, when analysed across all
403 cross types and all time points (Wilcoxon rank sum test with continuity correction; W = 1395.5, p =
404 0.046; **Figure 4**, top left hand boxplot). Analyzing cross types separately, the viability of offspring from
405 parallel-selected populations was significantly higher than the viability of hybrids made from divergent-
406 selected parents in two of the three cross types, when averaged across all time points (Kruskal-Wallis:
407 NaCl x EtOH: $X^2 = 7.6216$, p = 0.022; NaCl x LiAc0.02: $X^2 = 14.209$, p = 0.001). In the NaCl x LiAc0.01 cross
408 type, the viability between parallel-selected populations was similar to that between divergent-selected
409 populations ($X^2 = 5.834$, p = 0.054).

410 Following the breakdown of hybrid viability over time, the viability between divergent-selected
411 parents was still relatively high at early time points of divergence (on average 89.1% ± 0.02 at 100
412 generations), but then decreased substantially between 250 and 500 generations to on average 66% ±
413 0.08 (**Figure 4**, top left hand line plot) below that of parallel-selected crosses. This pattern was not
414 consistent among all cross types. The viability of two parallel-selected cross types (LiAc0.01 x LiAc0.01,
415 EtOH x EtOH) was higher than that of the divergent-selected crosses on average (although not all within-
416 time point comparisons were significant), but a notable exception were the crosses made between the
417 parallel-selected LiAc0.02 x LiAc0.02 populations, which dropped in viability after 500 generations, to a
418 similar extent as that of the divergent-selected NaCl x LiAc0.02 hybrids. We discuss potential
419 explanations for this below.

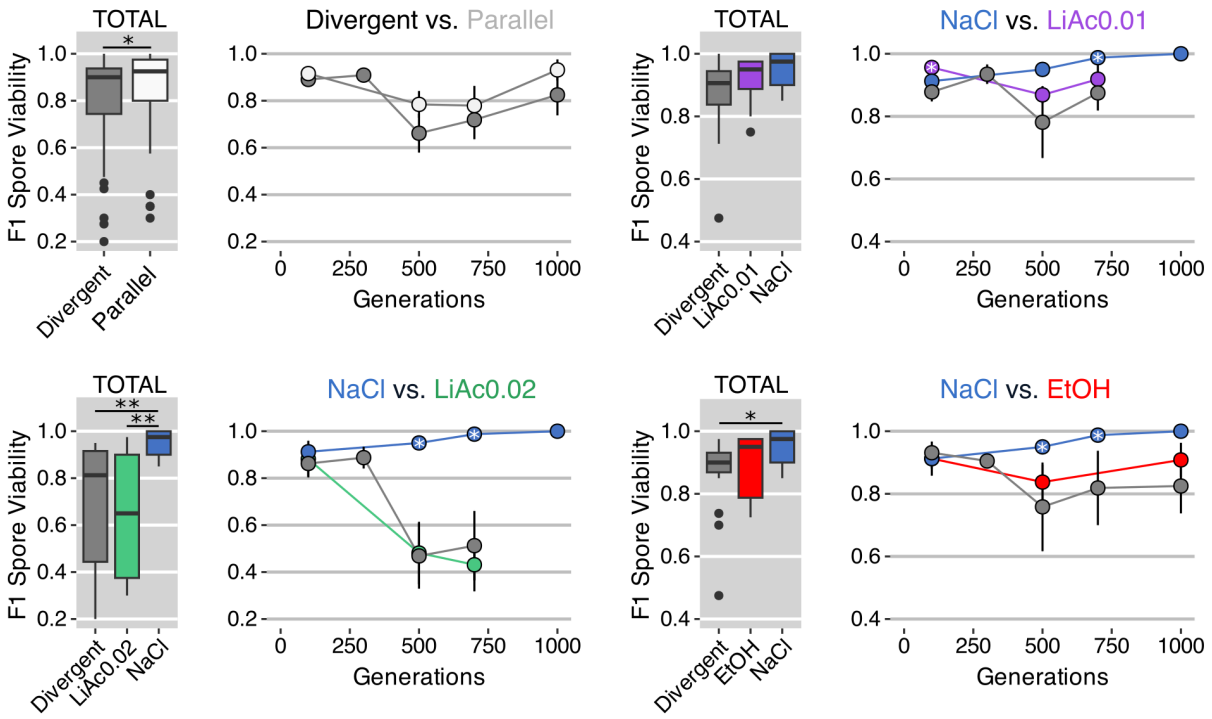

Figure 4: Analysis of reproductive isolation. The viability of F1 spores (i.e. the recombined haploid F2 offspring), which is an inverse measure of reproductive isolation, at five time points (number of generations) of experimental evolution. Circles indicate the mean measurement and the vertical line indicates the standard error of the mean. Crosses made between parallel-selected populations evolving in the same environment are coloured (or white in the top left hand plot), crosses made between divergent-selected populations, evolving in different environments, are grey. Box plots show means (thick horizontal line) across all generations of each cross type. 'Divergent' are the crosses between divergent-selected populations (NaCl vs LiAc0.01, NaCl vs LiAc0.02, NaCl vs EtOH). Black asterisks indicate statistical significance using Kruskal-Wallis and pairwise Wilcoxon post hoc tests with Bonferroni correction (adjusted $p < 0.001$ = ***, < 0.01 = **, < 0.05 = *). White asterisks inside circles indicate significantly lower viability in divergent- than in parallel-selected crosses, using one-sided Wilcoxon tests with Bonferroni corrections (adjusted $p < 0.05$ = *).

The genome-wide mutational landscape of adaptation and hybridization

In an effort to find the genetic mechanisms potentially underlying postzygotic reproductive isolation, we assessed the genome-wide mutational landscape of the divergent-evolved parental populations, and the F1 and F2 hybrid crosses made between them, at all seven sampled timepoints. We focused on three major mutational classes: single nucleotide variants (SNVs), large structural variants (SVs), and copy number variants (CNVs).

440 As might be expected from selective sweeps during directional selection, we found that all
441 populations showed reduced SNV mutational diversity compared to the founder population within the
442 first 100 generations of evolution (dashed black lines in Figure S3A). Most identified mutations were
443 single nucleotide variants, fewer were insertions and deletions (indels) (Figure S4). The mutational SNV
444 load in LiAc0.02 populations was consistently lower than in populations evolving in NaCl and in their F1
445 and F2 hybrids, and remained low through time (Kruskal-Wallis: $X^2 = 44.95$, $p < 0.001$, Figure S3A). This
446 pattern remained after filtering for mutational variants estimated by SnpEff to have high impact
447 (Kruskal-Wallis: $X^2 = 13.07$, $p=0.004$, **Figure 5A**). LiAc0.02 populations also showed a lower SNV
448 mutational load than the populations evolving in the weaker concentration of lithium acetate (LiAc0.01).
449 It is possible that this is the result of stronger purifying selection in LiAc0.02 populations from the start.
450 But since populations evolving in the stronger concentration of lithium acetate have likely also
451 undergone fewer mitotic generations, this may also reflect mutations accumulating primarily as a
452 function of reproductive time. In the other three parental population types (NaCl, LiAc0.01 and EtOH),
453 SNV mutational load decreased over time (**Figure 5B**) and the pattern stayed consistent when filtering
454 for only mutations with high impact on fitness (Figure S5A). Conversely, in the F1 ($R = 0.48$, $p < 0.01$, in
455 grey) and F2 hybrid populations ($R = 0.57$, $p < 0.01$, in yellow), we found a total increase in mutational
456 load over time (**Figure 5B**). Thus, the more the parental populations diverged phenotypically and
457 genetically over time, the more single nucleotide mutational variants were detected in their resulting F1
458 and F2 hybrid populations.

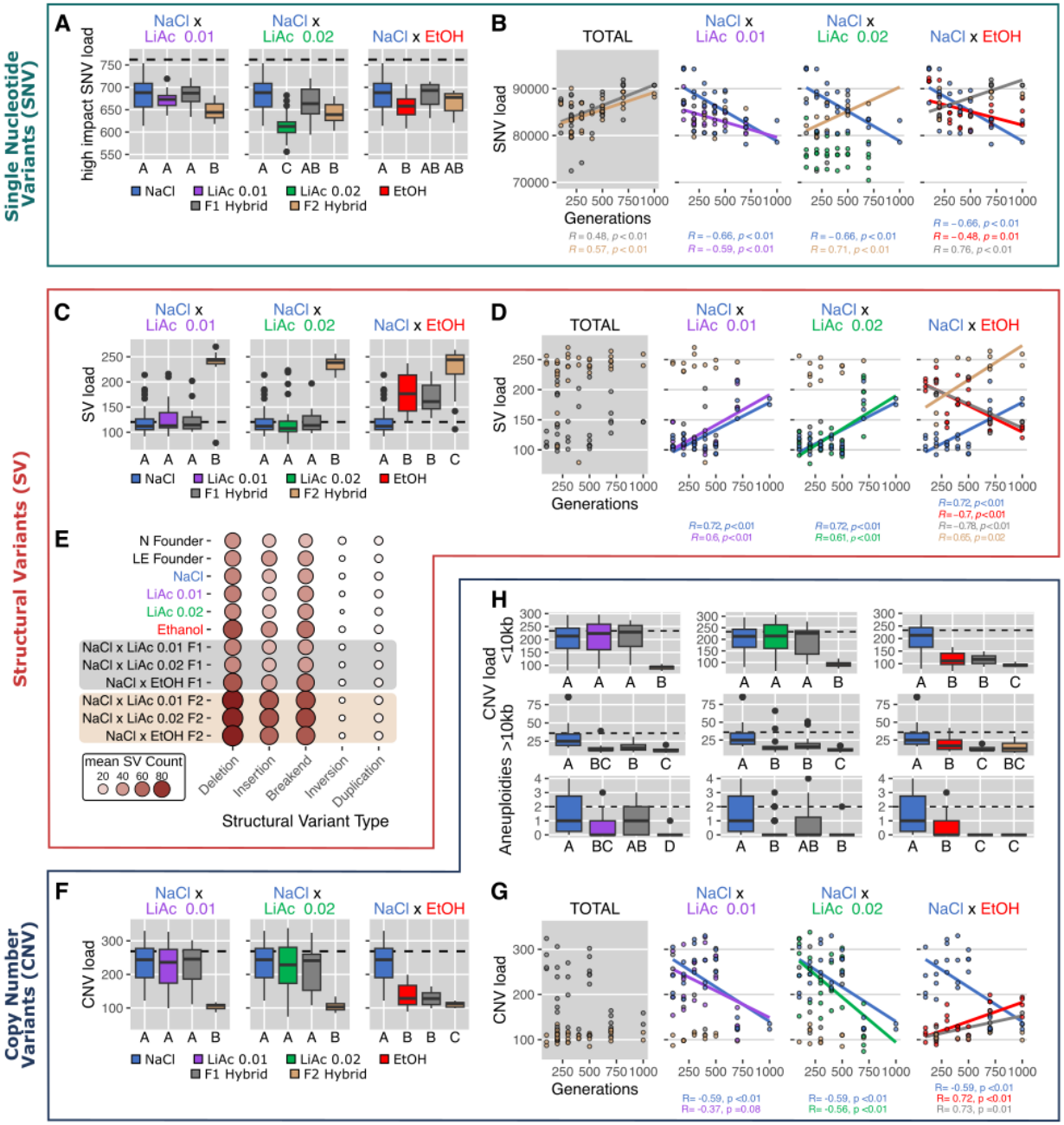

Figure 5: The genome-wide mutational landscape of hybridization at seven time points of experimental evolution. **A)** Single nucleotide variant (SNV) mutational load after filtering for high impact mutations on gene function using SnpEff v5.2 (Cingolani et al. 2012). The mutational load is averaged across all timepoints for each hybrid cross. The mean mutational load of the founder population is indicated by the dashed black line. Boxplots indicate the first and third quartiles with whiskers extending to the furthest point not exceeding 1.5 x the interquartile range and outliers beyond this are shown as dots. The solid line indicates the median value. Different letters (A, B and C) indicate statistically significant differences using Kruskal-Wallis and pairwise Wilcoxon post hoc tests with Bonferroni corrections. **B)** Linear regression (Pearson R) of SNV mutational load at seven time points (n of generations) of experimental evolution. Only significant linear relationships are shown ($p \leq 0.05$). The gray plot includes

470 F1 and F2 hybrids across all crosses. **C)** Structural variant (SV) mutational load averaged across all
471 sampled timepoints (TOTAL) for the three types of hybrid crosses. SV mutational load consists of the
472 number of deletions, insertions, inversions, tandem duplications and interchromosomal translocations
473 (> 8bp) detected in the population. Colors, boxplots, and statistical significance are consistent with panel
474 A. **D)** Linear regression (Pearson R) between SV mutational load and increasing timepoints of parental
475 divergence (number of generations). Only significant linear relationships are shown ($p \leq 0.05$). The gray
476 plot includes F1 and F2 hybrids from all crosses. **E)** Mean structural variant count of each type of
477 structural variant (deletion, insertion, breakend, inversion and duplication) for each environment and
478 cross. Node color and size indicates the mean count of each variant type across all timepoints. **F)** Copy
479 number variant (CNV) mutational load consisting of amplifications, deletions and aneuploidies. CNV
480 mutational load averaged across all sampled timepoints (TOTAL) for the three types of hybrid crosses.
481 Colors, boxplots, and statistical significance are consistent with panel A. **G)** Linear regression (Pearson R)
482 between CNV mutational load and increasing timepoints of parental divergence (number of
483 generations). Only significant linear relationships are shown ($p \leq 0.05$). The gray plot includes F1 and F2
484 hybrids from all crosses. **H)** The distribution of large (>10kb) CNVs, small (< 10kb) CNVs and chromosome
485 aneuploidy (> 60% amplified or deleted) across all sampled timepoints for the three types of hybrid
486 crosses. Colors, boxplots, and statistical significance are consistent with panel A.
487
488 Analysis of structural variants (i.e. insertions, deletions, duplications, inversions and
489 interchromosomal translocations that are > 8bp) showed that the total number of SVs found in the
490 evolving parental populations remained comparable to the levels in the founder population (dashed
491 black lines in **Figure 5C**). Unlike the pattern we found in SNV mutational load, the number of SVs
492 harbored in parental populations increased over time (**Figure 5D**). This positive linear relationship was
493 consistent for populations evolving in NaCl ($R = 0.72$, $p < 0.01$), LiAc0.01 ($R = 0.6$, $p < 0.01$), and LiAc0.02
494 ($R = 0.61$, $p < 0.01$), but not for EtOH populations, which already had elevated levels of SVs ($p < 0.001$)
495 early on but then decreased over time ($R = -0.7$, $p < 0.01$; Figure S6A).
496 Strikingly, we found very high levels of SVs in all types of F2 hybrid crosses, right from the
497 beginning of parental population divergence (Kruskal-Wallis: NaCl x LiAc0.01: $X^2 = 22.87$, $p < 0.001$; NaCl x
498 LiAc0.02: $X^2 = 30.28$, $p < 0.001$; NaCl x EtOH: $X^2 = 34.45$, $p < 0.001$). In most cases, F2 hybrid populations
499 harboured almost twice as many structural variants compared to the corresponding parental
500 populations and the F1 hybrids. This pattern was seen across SV types collectively, but was particularly
501 prominent for insertions, deletions and interchromosomal translocations (breakend mutations, **Figure**

502 **5E**, Figure S7-S11). Duplications were rare compared to deletions and insertions and are therefore not
503 driving the elevated levels of SVs observed in F2 hybrid genomes (**Figure 5E**). Because F2 hybrids are
504 distinguished from F1 hybrids and the parent populations only by having passed through one round of
505 meiosis, the additional load of structural variants we found in F2 hybrids likely arose due to meiotic
506 errors.

507 In addition to structural variants, we also more comprehensively assessed copy number
508 variations (CNV) across the genome, which are a subtype of structural variation. In the structural
509 variation analysis, detection of variants was limited by the read pair fragment size. However, copy
510 number variants can range from small focal amplifications or deletions to chromosome arm, or whole
511 chromosome aneuploidies. Therefore, we used an approach that employs sequencing read depth and
512 allelic imbalances to estimate segmented copy number uniformly throughout the genome. On average,
513 parental populations, F1 and F2 hybrids had a lower CNV mutational load compared to the founder
514 population (dashed black lines in **Figure 5F**), suggesting that directional adaptation has reduced CNV
515 load in all environments. This pattern remained consistent when including the size of each copy number
516 variant to estimate the fraction of altered genome content (Figure S12B). Most populations showed
517 moderate levels (< 10%) of total alteration (amplification + deletion) of the genome by CNV (Figure
518 S12B). However, NaCl populations had a larger fraction of their genomes altered in copy number than
519 parental populations evolved in LiAc and EtOH (pairwise Wilcoxon test: vs LiAc0.01: $p < 0.001$; vs
520 LiAc0.02: $p < 0.001$; vs EtOH: $p = 0.012$). This is due to three parallel-evolved NaCl populations that had a
521 large fraction of genome alterations (> 20%) at three different time points of evolution.

522 Strikingly, the F2 hybrid genomes of all three crosses contained significantly fewer CNVs than
523 parental populations and most F1 hybrids (**Figure 5F**; Kruskal-Wallis: NaCl x LiAc0.01: $X^2 = 30.1$, $p <$
524 0.001; NaCl x LiAc0.02: $X^2 = 24.4$, $p < 0.001$; NaCl x EtOH: $X^2 = 37.7$, $p < 0.001$) and F2 hybrid genomes of
525 all crosses were significantly less altered by CNVs (in % genome) than the parental populations (Figure

526 S12B). Overall, we found that amplifications were more common than deletions across populations and
527 through time (Figure S13).

528 Similar to SNVs and SVs, we found consistent patterns of increase or decrease in CNVs with the
529 number of parental generations of evolution in divergent environments (**Figure 5G**). In the parental NaCl
530 ($R = -0.59$, $p < 0.01$) and LiAc0.02 ($R = -0.56$, $p < 0.01$) populations, the CNV mutational load decreased
531 with the number of generations. In the LiAc0.01 parents, the same pattern was seen but was not
532 significant ($R = -0.37$, $p = 0.08$). Interestingly, CNV mutational load was often relatively stable until
533 approximately 500 generations, followed by a steep decrease (**Figure 5G,** Figure S12A). In the EtOH
534 parents, we found the opposite pattern, with CNV load increasing with the number of generations
535 ($R=0.72$, $p <0.01$), affecting the F1 hybrid genomes between NaCl and EtOH in the same way ($R = 0.73$, p
536 $= 0.01$).

537 Lastly, we sought to understand if these patterns of CNV load were driven by small focal variants
538 or larger multi-kilobase alterations, including whole chromosomal aneuploidies. We found that the
539 majority of variants were small (< 10kb) and contributed significantly to the global pattern found in CNV
540 load (compare upper row of plots in **Figure 5H** to **Figure 5F**). A closer examination of the number of
541 larger alterations (> 10kb; middle row of plots in **Figure 5H**), revealed that the F2 hybrid genomes of two
542 hybrid crosses (NaCl x LiAc0.01, NaCl x LiAc0.02), showed significantly fewer large alterations (on
543 average 12.1) than their respective parents (on average 20.8) and F1 hybrids (on average 19.4). This
544 pattern is further emphasized when examining exclusively the number of aneuploid chromosomes
545 (>60% amplified or deleted) found in each sample (lower row of plots in **Figure 5H**). On average, F2
546 hybrid genomes carried fewer aneuploidies (mean=0.24 chromosomes) compared to parent
547 (mean=0.67) and F1 hybrid genomes (mean=0.64).
548

549 ***The distribution of mutational events across the genome***

550 After assessing the genome-wide mutational landscape in terms of SNVs, SVs, and CNV mutational load,
551 we determined the distribution of these mutational events across the genome. We found that the rate
552 of SNVs was not uniformly distributed, but instead showed chromosomal biases (Kruskal-Wallis: X^2 =
553 147.28, p <0.001, **Figure 6A**). Chromosomes VI and VIII had significantly higher frequencies of SNVs (16.7
554 and 14.1 mutations/kb, respectively). Chromosome I and IX also showed slightly elevated SNV
555 frequencies (10.8 and 9.35 mutations/kb, respectively). Chromosome VII on the other hand showed a
556 significantly lower frequency of SNVs (2.29 mutations/kb). The remaining chromosomes had
557 approximately equal frequencies of SNVs (6.39-7.34 mutations/kb). These chromosomal biases in SNV
558 distribution already existed in the founder population and remained consistent across all parental
559 lineages and all F1 and F2 hybrids (**Figure 6A**).

560 The distribution of structural variant (SV) events were also not uniformly distributed throughout
561 the genome (Kruskal-Wallis: X^2 = 60.06, p <0.001, **Figure 6B**). Similar to the SNV distribution, we found
562 highly elevated rates of SVs on chromosome VI (0.03 mutations/kb). We also found peaks in the rate of
563 SVs in chromosomes I, III, and IX in most parental and hybrid populations.

564 The proportion of whole chromosomes altered by copy number variants was not consistent
565 across environments and hybrid crosses (**Figure 6C**). Interestingly, F2 hybrids of all crosses showed the
566 lowest levels of copy number alterations, and aneuploidy (defined as > 60% of chromosome
567 amplification) was consistently rare across all F2 hybrid chromosomes. We discuss the implications of
568 the near absence of aneuploidies and large genome alterations in F2 hybrid genomes below. Our
569 analysis shows that the two founding populations each carried aneuploid chromosomes. The NaCl
570 founder population (N founder, **Figure 6C**) had an extra chromosome X, while the LE founder population
571 had three aneuploid chromosomes (I, III and VI). It is important to note that deeper analysis of
572 sequencing read depth of early generational timepoints from an earlier study (Ament-Velásquez et al.

573 2022) revealed that these aneuploidies were lost in the population within the first 30 or 60 generations
574 of adaptation (Figure S14). Parental NaCl populations subsequently lost the extra chromosome X over
575 the course of experimental evolution, but evolved an aneuploid chromosome I and underwent
576 alterations of large portions of chromosome III and VI. Chromosome I was also heavily altered in parent
577 populations evolving in LiAc 0.01 (40%), LiAc 0.02 (37%), and EtOH (25%). Similarly, F1 hybrid crosses
578 between NaCl and the two LiAc populations (to a lesser extent the NaCl x EtOH F1 hybrids) also showed
579 large copy number alterations in chromosomes I, III, and VI (**Figure 6C**). Confirming our previous result
580 (Ament-Velásquez et al. 2022), we also recovered a chromosome X aneuploidy in two parental EtOH
581 populations and the chromosome XI aneuploidy in one parental EtOH population here.

582 The 16 chromosomes of *S. cerevisiae* range widely in size from 270kb (chrVI) to 1,531kb (chrIV;
583 **Figure 6D**). As might be expected, larger chromosomes are larger targets for SNVs, SVs and CNVs and
584 therefore have higher overall mutational load for each mutational class. However, after correcting
585 mutational load for chromosome size, either by reporting SNVs and SVs as mutations per kilobase or
586 reporting CNVs as the percentage of chromosome altered, we found a strong negative relationship
587 between chromosome size and SNV, SV and CNV mutational rate (**Figure 6D**). Smaller chromosomes had
588 elevated rates of mutation while larger chromosomes were rarely affected. This pattern is most striking
589 in CNVs where, as previously mentioned, chromosomes I, III and VI were disproportionately altered. This
590 is interesting because chromosomes I, III, and VI are the smallest chromosomes in the yeast genome and
591 have been frequently reported to carry aneuploidies in other yeast studies as well (reviewed in (Gilchrist
592 and Stelkens 2019), likely because aneuploidies of smaller chromosomes cause fewer deleterious gene
593 dosage effects and can be compensated for at the proteome level (Muenzner et al. 2024). This pattern
594 of chromosome size bias for CNVs extends beyond intraspecific crosses and has been found across
595 interspecific yeast hybrids with diverse ancestries (Bendixsen, Peris, et al. 2021).

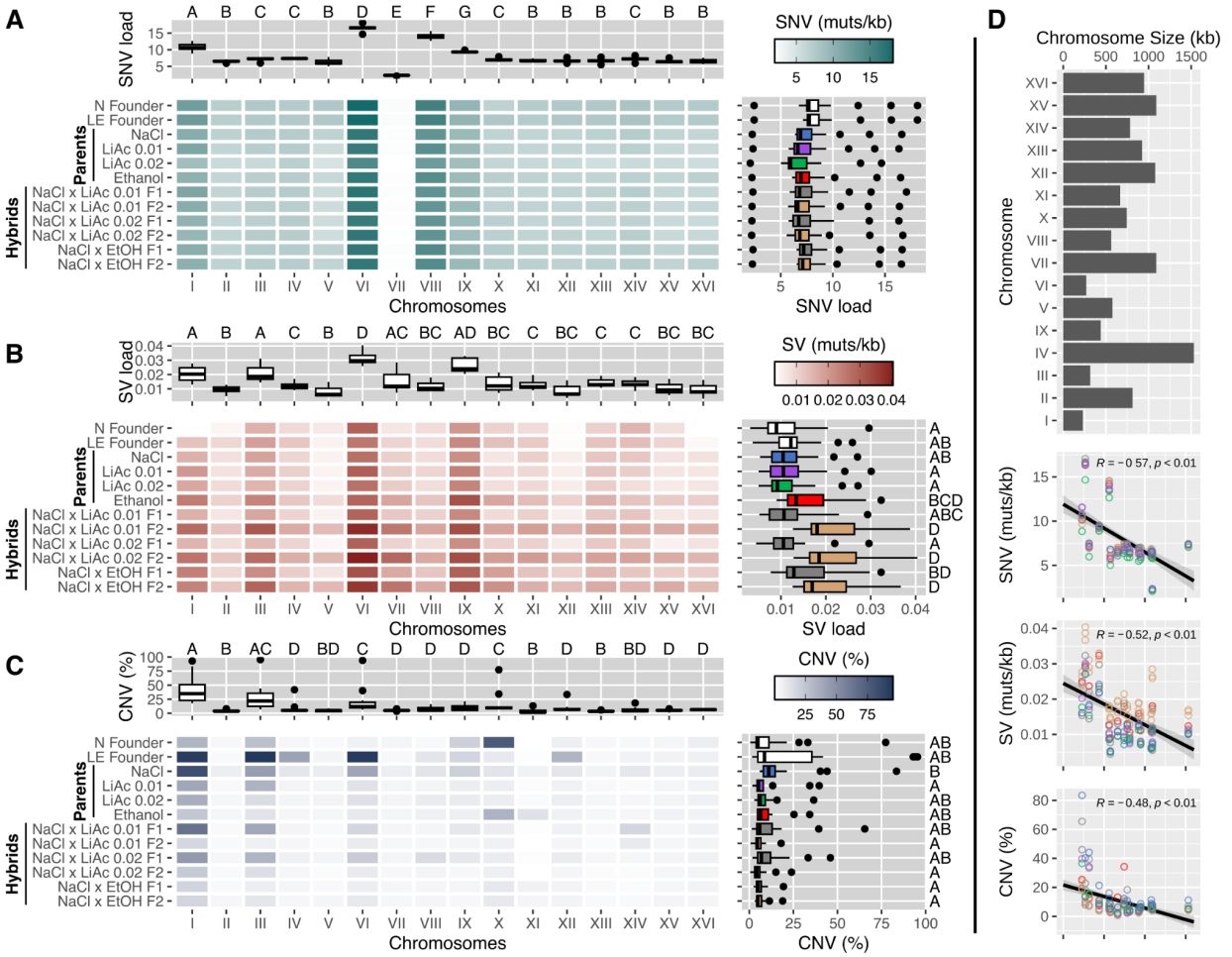

Figure 6: The distribution of mutational events across the genome. A) The mean number of events (mutations/kb) for each chromosome across all available timepoints. The top graph shows the distribution of mean SNV counts for each chromosome, while the right graph shows the distribution for each environment and hybrid cross. Boxplots indicate the first and third quartiles with whiskers extending to the furthest point not exceeding 1.5 x the interquartile range and outliers beyond this are shown as dots. The solid line indicates the median value. Different letters (A, B, C, D) indicate statistically significant differences using Kruskal-Wallis and pairwise Wilcoxon post hoc tests with Bonferroni corrections. **B)** The mean number of structural variant (SV) events (mutations/kb). **C)** The mean amount of genome altered (%) by copy number variants (losses and gains), including whole chromosome aneuploidies. **D)** The relationship between chromosome size and SNVs, SVs or CNVs. The barplot indicates the size of each of the 16 chromosomes in *Saccharomyces cerevisiae* reported in kilobases. The linear correlations show the mean SNV (muts/kb), SV (muts/kb) or CNV (% genome altered) for each population and for each chromosome as shown in the top graphs of panels A, B and C. The colors of each node indicate the populations (NaCl, LiAc0.01, LiAc0.02, EtOH, Hybrid F1, Hybrid F2).

611

612 **Discussion**

613 We used experimental evolution with budding yeast to test for the evolution of reproductive isolation as
614 a result of ecologically divergent selection, a process called ecological speciation (Mayr 1947; Schluter
615 2001; McKinnon et al. 2004; Nosil 2012; Jarrett et al. 2025). Previous studies with yeast have tested for
616 reproductive isolation between species that have diverged millions of years ago, which translates into
617 billions of generations (Greig et al. 2002; Shapira et al. 2014; Stelkens et al. 2014; Bernardes et al. 2017;
618 Eberlein et al. 2019; Gallone et al. 2019; Zhang et al. 2020; Bautista et al. 2021; Brice et al. 2021;
619 Bautista et al. 2023). Here, instead of starting with already divergent species, separated by billions of
620 generations, each with a complex evolutionary history of selection, genetic drift, recombination, and
621 gene flow, we generated phenotypic and genetic divergence over only a few hundred generations. We
622 evolved replicate populations in allopatry, in four different environments, under both ecologically
623 divergent and parallel selection. Hence, we controlled the type and degree of selection, minimized
624 genetic drift and recombination, and excluded gene flow. We systematically produced hybrid crosses
625 between these populations at increasing time points of experimental evolution, to test whether
626 reproductive isolation evolved between the divergent-selected populations, as predicted by ecological
627 speciation theory.

628

629 ***Divergent ecological selection leads to partial reproductive isolation***

630 First, we confirmed that populations when evolved in different environments, increasingly diverged in
631 phenotypic traits that were not directly under selection. The parallel-selected (control) populations on
632 the other hand remained phenotypically similar (**Figure 2**). This provides evidence for large scale
633 phenotypic differentiation under divergent selection. Second, the genomes of divergent-selected
634 populations became more genetically differentiated over time, showing higher F_{st} - values and lower

635 similarity (Jaccard index) than those of the parallel-selected populations (**Figure 3**). Third, we found that
636 divergent-selected populations produced hybrid gametes with reduced viability, which is a classic
637 signature of postzygotic reproductive isolation in the form of hybrid breakdown (**Figure 4**). Zygotes
638 generated from parallel-selected populations on the other hand remained reproductively more
639 compatible, with some exceptions (**Figure 4**). Together, our results suggest that partial reproductive
640 isolation evolved due to divergent ecological selection in our experiment. Alternative processes, such as
641 mutation-order effects (Schluter 2009; Ono et al. 2017), may have contributed to the build up of
642 reproductive barriers, but since most parallel-selected populations remained compatible, neither the
643 timing nor the order in which mutations occurred likely played a large role.
644
645 ***Recombination errors may cause genomic instability in hybrids***
646 Early experiments, e.g. in fruit flies with similar set-ups of divergent- and parallel-selected lines on
647 different media (Dodd 1989) and a large body of theory (reviewed in Kirkpatrick and Ravigné 2002) have
648 demonstrated the evolution of reproductive isolation as a consequence of adaptive divergence (Nosil
649 2012). Here, we have taken additional steps to understand the genetic basis of this hybrid breakdown.
650 Our population genomic analyses show that, as parental populations diverged phenotypically and
651 genetically over time, the mutational load of single nucleotide variants (SNVs) steadily increased in F1
652 and F2 hybrids (**Figure 5B)**, with a bias for chromosomes I, VI, and VIII (**Figure 6A**). We speculate that the
653 sudden breakdown of hybrid viability between 250 and 500 generations (**Figure 4**) may be a threshold
654 effect of mutational load, where mutations have only small, non-linear effects on viability until a critical
655 point is reached, after which DNA repair pathways are increasingly defective in hybrid genomes.
656 Even more strikingly, F2 hybrid populations harboured more than twice as many structural
657 variants (SVs) than their respective parental populations and the F1 hybrids. This pattern was seen
658 across all SV types (**Figure 5C**), but was particularly strong for insertions, deletions, and

659 interchromosomal translocations (breakend mutations, Figure S7-S11) with strong chromosomal biases
660 for chromosomes I, III, VI, and IX (**Figure 6B**). Because F2 hybrids differ from F1 hybrids only by one
661 meiotic event (and a few mitotic generations before and after sporulation that are negligible), the
662 increase in structural variants seen in F2 hybrids can only reasonably be explained by errors during
663 meiosis. This suggests that ecological divergence has led to hybrid offspring with higher genomic
664 instability due to meiotic recombination errors (e.g. unequal or incorrect crossing overs), resulting in
665 frequent chromosomal rearrangements (SVs). However, additional sequencing data from crosses
666 between parallel-selected populations (not available to us yet) would be needed for comparison, to
667 conclusively test for causality between divergent selection and genome instability.
668 Interestingly, F2 hybrids showed the lowest levels of copy number alterations, and aneuploidy
669 rates were consistently low across all chromosomes in F2 hybrid genomes (**Figure 5F, Figure 6C**).
670 Meanwhile, all parent and F1 hybrid populations contained various aneuploidies, especially in
671 chromosomes I, III, and VI, which are the smallest chromosomes in the yeast genome and frequently
672 reported to carry aneuploidies (reviewed in Gilchrist and Stelkens 2019). Note, that the aneuploidies
673 originally present in the founder populations (Figure S14) had disappeared from the evolving parental
674 populations before we made the first hybrid cross at 100 generations, hence all aneuploidies arose *de*
675 *novo* over the course of experimental evolution, or after meiosis in the F2 genomes. The absence of
676 aneuploidies in F2 hybrids is surprising and contrasts with the high SV load found in hybrid genomes. We
677 expected errors during meiosis to also lead to increased chromosome non-disjunction and aneuploidy. A
678 plausible explanation is that, by default, we only sequenced viable genotypes that had successfully
679 passed through meiosis and germinated. Average mortality due to lethal aneuploidies is likely high in the
680 recombined haploid gametes, where copy number imbalances imposed by aneuploidies are more
681 pronounced, and lethality has additional opportunities to manifest when strains are pushed through

682 germination. As a result, aneuploidies may have been efficiently purged from F2 hybrid genomes before
683 the sequencing stage.
684
685 ***A putative genetic mechanism for reproductive isolation***
686 Experimental and genetic work in interspecific yeast crosses, made from species separated by billions of
687 generations and high nucleotide divergence (>10%), has shown that the main reason for hybrid
688 breakdown in yeast is antirecombination (Hunter et al. 1996; Rogers et al. 2018; Bozdag et al. 2021).
689 Antirecombination suppresses crossovers during meiosis when nucleotide divergence along
690 chromosomes is too high. The ensuing mispairing of homologous chromosomes causes missegregation
691 into the hybrid gametes, leading to lethal aneuploidies and typically > 90% spore mortality in
692 interspecific yeast crosses. This process has also been shown to cause hybrid sterility in mice, where it is
693 controlled by the Prdm9 gene (Forejt and Jansa 2023). However, antirecombination due to genome-
694 wide nucleotide divergence is unlikely to have played a role in the hybrid breakdown we observed here,
695 given the short evolutionary time span of our experiment. Instead, we suggest that the following
696 process underlies the build-up of reproductive barriers here: First, divergent ecological selection in the
697 parent populations has led to SVs with positive (adaptive) fitness effects and additional neutral SVs
698 hitchhiking along with them. These parental SVs then interfered with hybrid meiosis, causing additional
699 SVs to emerge in the hybrid genomes, due to unequal or incorrect crossing over. Cumulatively, the high
700 SV load of the hybrid genomes then negatively affected gamete viability, germination, and colony
701 formation, disrupting cell function and homeostasis (Chang et al. 2013; Liu et al. 2022). In short, we
702 suggest that the most likely genetic mechanism underlying hybrid breakdown in our experiment is the
703 high structural variant load of the hybrid genomes, which was jump-started by the increasing number of
704 SVs accumulating in the divergent-selected parent populations (**Figure 5D**). Whether the accumulation

705 of SVs in parent populations under divergent selection may be a common mechanism leading to
706 genomic instability in hybrids needs to be tested in other species and systems.

707 We found an interesting exception in crosses between parallel-selected LiAc0.02 populations
708 where, against our expectations, gamete viability decreased over time (**Figure 4**). We previously found
709 that three of four replicate populations evolving in LiAc0.02 had turned (functionally) haploid early on in
710 experimental evolution (Ament-Velásquez et al. 2022). In haploid populations, beneficial mutations can
711 sweep to fixation faster and deleterious mutations are more quickly purged by purifying selection, as
712 they are not masked by heterozygosity (Gerstein et al. 2011; Cervantes et al. 2023). This is consistent
713 with our finding that the mutational SNV load in LiAc0.02 populations was consistently lower than in
714 other populations, which may be the result of stronger purifying selection in this environment. These
715 processes are particularly efficient in large populations exposed to stressful environments with strong
716 selection, which the LiAc0.02 environment represents (Ament-Velásquez et al. 2022). Propelled by
717 clonal interference, this may have affected the adaptive dynamics (the rate and direction of allele
718 frequency changes) in the LiAc0.02 populations in idiosyncratic ways, leading to substantial genetic
719 differentiation and incompatibilities between them, despite parallel selection pressures.

720 Although we may speculate on the mechanisms causing reproductive isolation in our
721 experiment, the underlying genetic architecture of reproductive isolation remains unidentified. The
722 pattern of decreasing genomic similarity and increasing F_{st} between divergent-selected populations
723 (while parallel-selected populations remained similar), and the vast genome-wide instability found in
724 hybrid genomes, does suggest that reproductive isolation is based on (or at least accompanied by)
725 multiple genomic regions and that 'continents' rather than 'islands' of differentiated loci are operating
726 together (Michel et al. 2010). However, due to the absence of sexual recombination during the
727 evolution of the parent populations in our experiment, other evolutionary mechanisms may have also
728 caused large genomic regions to become differentiated. Effects of clonal interference and linked

729 selection for example, i.e. the competition between multiple beneficial mutations arising independently
730 in the same population leading to only one lineage sweeping through the population, may have caused
731 genetic differentiation between populations that is not due to ecological selection alone. Although our
732 previous work has identified the number and types of adaptive mutations segregating and fixing in the
733 evolving parental populations (Ament-Velásquez et al. 2022), our pool-seq approach does not provide
734 haplotype information. Thus, we cannot infer which and how many genes are causing reproductive
735 isolation, how large their effect sizes are, and whether they are genomically clustered (Nosil and Feder
736 2012). Directed crosses between parents with known genotypes, and dissecting and genotyping a large
737 number of recombined F2 gametes, could identify incompatible chromosomes, chromosomal regions, or
738 individual genes causing reproductive isolation in this system.
739
740 ***Conclusions***
741 Selection against hybrids due to ecological factors, when hybrid phenotypes are ill-adapted to existing
742 ecological niches, has often been considered as being different from selection arising from epistatic
743 (Dobzhansky-Muller) incompatibilities (Thompson et al. 2023). There is a recent push to close this gap
744 between evolutionary ecology and speciation genetics, and to focus more on the role of the
745 environment and ecological adaptation in driving what we traditionally think of as 'intrinsic' genetic
746 isolation barriers (Anderson et al. 2023; Thompson et al. 2023). Our study contributes to bridging this
747 gap by synthesizing phenotypic and whole genome data, and demonstrating that divergent ecological
748 adaptation can indeed promote intrinsic reproductive isolation, consistent with predictions of ecological
749 speciation theory. Our population genomics results show that divergent ecological selection, even for
750 relatively few mitotic generations, was accompanied by vast genomic instability in F2 hybrids, including
751 deletions, inversions, and interchromosomal translocations. Our multifaceted approach of combining
752 experimental evolution with sexual microbes, hybridization at increasing time points of divergence,

high-throughput phenotyping, and comparative genomics, confirms the ability of ecology to drive reproductive isolation and speciation. Our approach can be further developed to provide a comprehensive empirical framework to test different concepts in speciation research. This includes, for instance, i) testing if the speciation continuum is a 'continuum of reproductive isolation' (Stankowski and Ravinet 2021) and whether reproductive isolation barriers accumulate linearly or, as predicted by theory, exponentially (Orr 1995), the 'missing snowball' controversy); ii) testing if the 'speciation hypercube' captures the complexity of species divergence (Dieckmann et al. 2004; Bolnick et al. 2023), by including more phenotypic and genetic variables, and iii) to better understand the evolution of hybrid fitness during speciation by including additional data sets (e.g. gene interaction networks (Dagilis et al. 2019), which could reconcile the contrasting outcomes of epistatic genetic interactions leading to hybrids with both increased (heterosis) and decreased fitness (hybrid inviability) during different stages of speciation.

Acknowledgements

We thank Maria de la Paz Celorio Mancera, Viktoria Köppä, and Zebin Zhang for helping with serial transfers and media preparation, and Lorena Ament-Velásquez for bioinformatics advice. We also thank three anonymous reviewers for their constructive comments on an earlier draft. Computation was performed on resources provided by SNIC through Uppsala Multidisciplinary Center for Advanced Computational Science (UPPMAX) under Projects NAISS2023/23-519 (Small Storage) and NAISS2023/22-62 and NAISS2023/22-924 (Small Compute). We acknowledge support from Science for Life Laboratory, the National Genomics Infrastructure, NGI, and Uppmax for providing assistance in massive parallel sequencing and computational infrastructure. This work was supported by Swedish Research Council Project Grants (2022-03427 to R.S. and 2022-03024 to J.W.), a Knut and Alice Wallenberg Foundation Grant (2017.0163 to R.S.), and the Wenner-Gren Foundations (UPD2018-0196, UPD2019-0110 to D.B.).

References

Alalam H, Graf FE, Palm M, Abadikhah M, Zackrisson M, Boström J, Fransson A, Hadjineophytou C, Persson L, Stenberg S, et al. 2020. A High-Throughput Method for Screening for Genes Controlling Bacterial Conjugation of Antibiotic Resistance. *mSystems* 5:e01226-20.

Ament-Velásquez SL, Gilchrist C, Rêgo A, Bendixsen DP, Brice C, Grosse-Sommer JM, Rafati N, Stelkens R. 2022. The Dynamics of Adaptation to Stress from Standing Genetic Variation and de novo Mutations. *Molecular Biology and Evolution* 39:msac242.

Anderson SAS, López-Fernández H, Weir JT. 2023. Ecology and the Origin of Nonephemeral Species. *The American Naturalist* 201:619–638.

Anderson SAS, Weir JT. 2022. The role of divergent ecological adaptation during allopatric speciation in vertebrates. *Science* 378:1214–1218.

Andrews S. 2010. FastQC: A Quality Control tool for High Throughput Sequence Data. Available from: https://www.bioinformatics.babraham.ac.uk/projects/fastqc/

Bautista C, Gagnon-Arsenault I, Utrobina M, Fijarczyk A, Bendixsen DP, Stelkens R, Landry C. 2023. Hybrid adaptation is hampered by Haldane's sieve. *bioRxiv*:2023–12.

Bautista C, Marsit S, Landry CR. 2021. Interspecific hybrids show a reduced adaptive potential under DNA damaging conditions. *Evolutionary Applications* 14:758–769.

Bell G, Gonzalez A. 2011. Adaptation and Evolutionary Rescue in Metapopulations Experiencing Environmental Deterioration. *Science* 332:1327–1330.

Belleau P, Deschênes A, Beyaz S, Tuveson DA, Krasnitz A. 2021. CNVMetrics package: Quantifying similarity between copy number profiles. *F1000Research* [Internet] 10. Available from: https://f1000research.com/slides/10-737

Bendixsen DP, Gettle N, Gilchrist C, Zhang Z, Stelkens R. 2021. Genomic Evidence of an Ancient East Asian Divergence Event in Wild Saccharomyces cerevisiae. *Genome Biology and Evolution* 13:evab001.

Bendixsen DP, Peris D, Stelkens R. 2021. Patterns of Genomic Instability in Interspecific Yeast Hybrids With Diverse Ancestries. *Frontiers in Fungal Biology* [Internet] 2. Available from: https://www.frontiersin.org/article/10.3389/ffunb.2021.742894

Bernardes JP, Stelkens RB, Greig D. 2017. Heterosis in hybrids within and between yeast species. *J Evol Biol* 30:538–548.

Boeva V, Popova T, Bleakley K, Chiche P, Cappo J, Schleiermacher G, Janoueix-Lerosey I, Delattre O, Barillot E. 2012. Control-FREEC: a tool for assessing copy number and allelic content using next-generation sequencing data. *Bioinformatics* 28:423–425.

811 Boeva V, Zinovyev A, Bleakley K, Vert J-P, Janoueix-Lerosey I, Delattre O, Barillot E. 2011. Control-free
812 calling of copy number alterations in deep-sequencing data using GC-content normalization.
813 *Bioinformatics* 27:268–269.

814 Bolger AM, Lohse M, Usadel B. 2014. Trimmomatic: a flexible trimmer for Illumina sequence data.
815 *Bioinformatics* 30:2114–2120.

816 Bolnick DI, Hund AK, Nosil P, Peng F, Ravinet M, Stankowski S, Subramanian S, Wolf JBW, Yukilevich R.
817 2023. A multivariate view of the speciation continuum. *Evolution* 77:318–328.

818 Bozdag GO, Ono J, Denton JA, Karakoc E, Hunter N, Leu J-Y, Greig D. 2021. Breaking a species barrier by
819 enabling hybrid recombination. *Current Biology* 31:R180–R181.

820 Brice C, Zhang Z, Bendixsen D, Stelkens R. 2021. Hybridization Outcomes Have Strong Genomic and
821 Environmental Contingencies. *The American Naturalist* 198:E53–E67.

822 Cervantes S, Kesälahti R, Kumpula TA, Mattila TM, Helanterä H, Pyhäjärvi T. 2023. Strong Purifying
823 Selection in Haploid Tissue–Specific Genes of Scots Pine Supports the Masking Theory.
824 *Molecular Biology and Evolution* 40:msad183.

825 Chang S-L, Lai H-Y, Tung S-Y, Leu J-Y. 2013. Dynamic Large-Scale Chromosomal Rearrangements Fuel
826 Rapid Adaptation in Yeast Populations. *PLOS Genetics* 9:e1003232.

827 Chen X, Schulz-Trieglaff O, Shaw R, Barnes B, Schlesinger F, Källberg M, Cox AJ, Kruglyak S, Saunders CT.
828 2016. Manta: rapid detection of structural variants and indels for germline and cancer
829 sequencing applications. *Bioinformatics* 32:1220–1222.

830 Cingolani P, Platts A, Wang LL, Coon M, Nguyen T, Wang L, Land SJ, Lu X, Ruden DM. 2012. A program for
831 annotating and predicting the effects of single nucleotide polymorphisms, SnpEff: SNPs in the
832 genome of Drosophila melanogaster strain w1118; iso-2; iso-3. *Fly (Austin)* 6:80–92.

833 Dagilis AJ, Kirkpatrick M, Bolnick DI. 2019. The evolution of hybrid fitness during speciation. *PLOS*
834 *Genetics* 15:e1008125.

835 Danecek P, Auton A, Abecasis G, Albers CA, Banks E, DePristo MA, Handsaker RE, Lunter G, Marth GT,
836 Sherry ST, et al. 2011. The variant call format and VCFtools. *Bioinformatics* 27:2156–2158.

837 Danecek P, Bonfield JK, Liddle J, Marshall J, Ohan V, Pollard MO, Whitwham A, Keane T, McCarthy SA,
838 Davies RM, et al. 2021. Twelve years of SAMtools and BCFtools. *GigaScience* 10:giab008.

839 Deschênes A, Belleau P, Tuveson DA, Krasnitz A. 2022. Quantifying similarity between copy number
840 profiles with CNVMetrics package. *F1000Research* [Internet] 11. Available from:
841 https://f1000research.com/posters/11-816

842 Dettman JR, Anderson JB, Kohn LM. 2008. Divergent adaptation promotes reproductive isolation among
843 experimental populations of the filamentous fungus Neurospora. *BMC Evol Biol* 8:35.

844 Dettman JR, Sirjusingh C, Kohn LM, Anderson JB. 2007. Incipient speciation by divergent adaptation and
845 antagonistic epistasis in yeast. *Nature* 447:585–588.

deVicente MC, Tanksley SD. 1993. Qtl Analysis of Transgressive Segregation in an Interspecific Tomato Cross. *Genetics* 134:585–596.

Dieckmann U, Doebeli M, Metz JAJ, Tautz D eds. 2004. Adaptive Speciation. Cambridge: Cambridge University Press Available from: https://www.cambridge.org/core/books/adaptive-speciation/A2413E0B1E5DDAB5C5848F0666468A35

Dodd DMB. 1989. Reproductive Isolation as a Consequence of Adaptive Divergence in Drosophila pseudoobscura. *Evolution* 43:1308–1311.

Eberlein C, Hénault M, Fijarczyk A, Charron G, Bouvier M, Kohn LM, Anderson JB, Landry CR. 2019. Hybridization is a recurrent evolutionary stimulus in wild yeast speciation. *Nat Commun* 10:923.

Filchak KE, Roethele JB, Feder JL. 2000. Natural selection and sympatric divergence in the apple maggot Rhagoletis pomonella. *Nature* 407:739–742.

Forejt J, Jansa P. 2023. Meiotic Recognition of Evolutionarily Diverged Homologs: Chromosomal Hybrid Sterility Revisited. *Molecular Biology and Evolution* 40:msad083.

Funk DJ, Nosil P, Etges WJ. 2006. Ecological divergence exhibits consistently positive associations with reproductive isolation across disparate taxa. *Proceedings of the National Academy of Sciences* 103:3209–3213.

Gallone B, Steensels J, Mertens S, Dzialo MC, Gordon JL, Wauters R, Theßeling FA, Bellinazzo F, Saels V, Herrera-Malaver B, et al. 2019. Interspecific hybridization facilitates niche adaptation in beer yeast. *Nat Ecol Evol* 3:1562–1575.

Garrison E, Marth G. 2012. Haplotype-based variant detection from short-read sequencing. *arXiv* 1207.

Gautier M, Vitalis R, Flori L, Estoup A. 2022. f-Statistics estimation and admixture graph construction with Pool-Seq or allele count data using the R package poolfstat. *Mol Ecol Resour* 22:1394–1416.

Gerstein AC, Cleathero LA, Mandegar MA, Otto SP. 2011. Haploids adapt faster than diploids across a range of environments. *Journal of Evolutionary Biology* 24:531–540.

Gilchrist C, Stelkens R. 2019. Aneuploidy in yeast: Segregation error or adaptation mechanism? *Yeast* 36:525–539.

Good BH, McDonald MJ, Barrick JE, Lenski RE, Desai MM. 2017. The dynamics of molecular evolution over 60,000 generations. *Nature* 551:45–50.

Gorter FA, Derks MF, van den Heuvel J, Aarts MG, Zwaan BJ, de Ridder D, de Visser JAG. 2017. Genomics of adaptation depends on the rate of environmental change in experimental yeast populations. *Molecular Biology and Evolution* 34:2613–2626.

Gorter FA, Scanlan PD, Buckling A. 2016. Adaptation to abiotic conditions drives local adaptation in bacteria and viruses coevolving in heterogeneous environments. *Biol. Lett.* 12:20150879.

Grant RB, Grant PR. 2003. What Darwin's Finches Can Teach Us about the Evolutionary Origin and

Regulation of Biodiversity. *BioScience* 53:965–975.

Greig D, Louis EJ, Borts RH, Travisano M. 2002. Hybrid Speciation in Experimental Populations of Yeast. *Science* 298:1773–1775.

Härer A, Bolnick DI, Rennison DJ. 2021. The genomic signature of ecological divergence along the benthic-limnetic axis in allopatric and sympatric threespine stickleback. *Molecular Ecology* 30:451–463.

Hatfield T, Schluter D. 1999. ECOLOGICAL SPECIATION IN STICKLEBACKS: ENVIRONMENT-DEPENDENT HYBRID FITNESS. *Evolution* 53:866–873.

Hendry AP, Nosil P, Rieseberg LH. 2007. The speed of ecological speciation. *Functional Ecology* 21:455–464.

Hivert V, Leblois R, Petit EJ, Gautier M, Vitalis R. 2018. Measuring Genetic Differentiation from Pool-seq Data. *Genetics* 210:315–330.

Hunter N, Chambers SR, Louis EJ, Borts RH. 1996. The mismatch repair system contributes to meiotic sterility in an interspecific yeast hybrid. *EMBO J* 15:1726–1733.

Irestedt M, Müller I, Thörn F, Joseph L, Nylander J, Guinet B, Valk TV der, Jønsson K. Reticulate and hybrid speciation is promoted by environmental instability in an Indo-Pacific species complex of whistlers (Aves: Pachycephala). Available from: https://www.authorea.com/doi/full/10.22541/au.173053090.08198521?commit=f442f52dffaefd5b78602e94558c1591a8dff4e5

Jarrett BJM, Downing PA, Svensson EI. 2025. Meta-analysis reveals that phenotypic plasticity and divergent selection promote reproductive isolation during incipient speciation. *Nat Ecol Evol* 9:833–844.

Johnson MS, Desai MM. 2022. Mutational robustness changes during long-term adaptation in laboratory budding yeast populations.Cooper VS, Walczak AM, Miller C, editors. *eLife* 11:e76491.

Kirkpatrick M, Ravigné V. 2002. Speciation by natural and sexual selection: models and experiments. *Am Nat* 159 Suppl 3:S22-35.

Kosheleva K, Desai MM. 2018. Recombination Alters the Dynamics of Adaptation on Standing Variation in Laboratory Yeast Populations. *Mol Biol Evol* 35:180–201.

Lenski RE, Rose MR, Simpson SC, Tadler SC. 1991. Long-Term Experimental Evolution in Escherichia coli. I. Adaptation and Divergence During 2,000 Generations. *The American Naturalist* 138:1315–1341.

Leu J-Y, Chang S-L, Chao J-C, Woods LC, McDonald MJ. 2020. Sex alters molecular evolution in diploid experimental populations of S. cerevisiae. *Nat Ecol Evol* 4:453–460.

Li H, Durbin R. 2009. Fast and accurate short read alignment with Burrows–Wheeler transform. *Bioinformatics* 25:1754–1760.

Li J, Vázquez-García I, Persson K, González A, Yue J-X, Barré B, Hall MN, Long A, Warringer J, Mustonen V, et al. 2019. Shared Molecular Targets Confer Resistance over Short and Long Evolutionary Timescales. *Molecular Biology and Evolution* 36:691–708.

Liu Y, Ma G, Gao Z, Li J, Wang J, Zhu X, Ma R, Yang J, Zhou Y, Hu K, et al. 2022. Global chromosome rearrangement induced by CRISPR-Cas9 reshapes the genome and transcriptome of human cells. *Nucleic Acids Research* 50:3456–3474.

Louder MIM, Justen H, Kimmitt AA, Lawley KS, Turner LM, Dickman JD, Delmore KE. 2024. Gene regulation and speciation in a migratory divide between songbirds. *Nat Commun* 15:98.

Mayr E. 1947. Ecological Factors in Speciation. *Evolution* 1:263–288.

McDonald MJ, Rice DP, Desai MM. 2016. Sex speeds adaptation by altering the dynamics of molecular evolution. *Nature* 531:233–236.

McKinnon JS, Mori S, Blackman BK, David L, Kingsley DM, Jamieson L, Chou J, Schluter D. 2004. Evidence for ecology's role in speciation. *Nature* 429:294–298.

Meyer JR, Dobias DT, Medina SJ, Servilio L, Gupta A, Lenski RE. 2016. Ecological speciation of bacteriophage lambda in allopatry and sympatry. *Science* 354:1301–1304.

Michel AP, Sim S, Powell THQ, Taylor MS, Nosil P, Feder JL. 2010. Widespread genomic divergence during sympatric speciation. *Proceedings of the National Academy of Sciences* 107:9724–9729.

Muenzner J, Trébulle P, Agostini F, Zauber H, Messner CB, Steger M, Kilian C, Lau K, Barthel N, Lehmann A, et al. 2024. Natural proteome diversity links aneuploidy tolerance to protein turnover. *Nature* 630:149–157.

Mukherjee V, Lind U, St. Onge RP, Blomberg A, Nygård Y. 2021. A CRISPR Interference Screen of Essential Genes Reveals that Proteasome Regulation Dictates Acetic Acid Tolerance in Saccharomyces cerevisiae. *mSystems* 6:10.1128/msystems.00418-21.

Müller I, Thörn F, Rajan S, Olsen R-A, Ericson P, Peona V, Smith B, Maiah G, Koane B, Iova B, et al. Ephemeral speciation in a New Guinean honeyeater complex (Aves: Melidectes). Available from: https://www.authorea.com/doi/full/10.22541/au.173639442.28305532?commit=c6fffa9cc0ca71d3e44f2de72f5001a07ea2ab20

Munar-Delgado G, Pulido F, Edelaar P. 2024. Performance-based habitat choice can drive rapid adaptive divergence and reproductive isolation. *Current Biology* 34:5564-5569.e4.

Nosil P. 2012. Ecological Speciation. Oxford University Press Available from: https://academic.oup.com/book/5499

Nosil P, Crespi BJ. 2006. Experimental evidence that predation promotes divergence in adaptive radiation. *Proceedings of the National Academy of Sciences* 103:9090–9095.

Nosil P, Feder JL. 2012. Genomic divergence during speciation: causes and consequences. *Philosophical Transactions of the Royal Society B: Biological Sciences* 367:332–342.

950 Nosil P, Schluter D. 2011. The genes underlying the process of speciation. *Trends Ecol Evol* 26:160–167.

951 Okonechnikov K, Conesa A, García-Alcalde F. 2016. Qualimap 2: advanced multi-sample quality control
952 for high-throughput sequencing data. *Bioinformatics* 32:292–294.

953 Ono J, Gerstein AC, Otto SP. 2017. Widespread Genetic Incompatibilities between First-Step Mutations
954 during Parallel Adaptation of Saccharomyces cerevisiae to a Common Environment. *PLOS*
955 *Biology* 15:e1002591.

956 Orr HA. 1995. The population genetics of speciation: the evolution of hybrid incompatibilities. *Genetics*
957 139:1805–1813.

958 Persson K, Onyema VO, Nwafor IP, Peri KVR, Otti C, Nnaemeka P, Onyishi C, Okoye S, Moneke A, Amadi
959 O, et al. 2024. Lactose-assimilating yeasts with high fatty acid accumulation uncovered by
960 untargeted bioprospecting. *Applied and Environmental Microbiology* 0:e01615-24.

961 Persson K, Stenberg S, Tamás MJ, Warringer J. 2022. Adaptation of the yeast gene knockout collection is
962 near-perfectly predicted by fitness and diminishing return epistasis. *G3*
963 *Genes|Genomes|Genetics* 12:jkac240.

964 Peter J, De Chiara M, Friedrich A, Yue J-X, Pflieger D, Bergström A, Sigwalt A, Barre B, Freel K, Llored A, et
965 al. 2018. Genome evolution across 1,011 Saccharomyces cerevisiae isolates. *Nature* 556:339–
966 344.

967 R Core Team. 2023. R: A Language and Environment for Statistical Computing. Available from:
968 https://www.R-project.org/

969 Rainey PB, Travisano M. 1998. Adaptive radiation in a heterogeneous environment. *Nature* 394:69–72.

970 Rice WR, Hostert EE. 1993. Laboratory Experiments on Speciation: What Have We Learned in 40 Years?
971 *Evolution* 47:1637–1653.

972 Rogers DW, McConnell E, Ono J, Greig D. 2018. Spore-autonomous fluorescent protein expression
973 identifies meiotic chromosome mis-segregation as the principal cause of hybrid sterility in yeast.
974 *PLOS Biology* 16:e2005066.

975 Rundle HD, Nagel L, Wenrick Boughman J, Schluter D. 2000. Natural selection and parallel speciation in
976 sympatric sticklebacks. *Science* 287:306–308.

977 Sawada A, Iwasaki T, Akatani K, Takagi M. 2022. Mate choice for body size leads to size assortative
978 mating in the Ryukyu Scops Owl Otus elegans. *Ecology and Evolution* 12:e9578.

979 Schluter D. 2001. Ecology and the origin of species. *Trends Ecol Evol* 16:372–380.

980 Schluter D. 2009. Evidence for Ecological Speciation and Its Alternative. *Science* 323:737–741.

981 Scopel EFC, Hose J, Bensasson D, Gasch AP. 2021. Genetic variation in aneuploidy prevalence and
982 tolerance across Saccharomyces cerevisiae lineages. *Genetics* 217:iyab015.

983 Shapira R, Levy T, Shaked S, Fridman E, David L. 2014. Extensive heterosis in growth of yeast hybrids is
984 explained by a combination of genetic models. *Heredity (Edinb)* 113:316–326.

985 Sparks MM, Kraft JC, Blackstone KMS, McNickle GG, Christie MR. 2022. Large genetic divergence
986 underpins cryptic local adaptation across ecological and evolutionary gradients. *Proceedings of*
987 *the Royal Society B: Biological Sciences* 289:20221472.

988 Stankowski S, Ravinet M. 2021. Defining the speciation continuum. *Evolution* 75:1256–1273.

989 Stelkens R. 2024. A microbial perspective on speciation. *Evolutionary Journal of the Linnean Society*
990 3:kzae023.

991 Stelkens RB, Brockhurst MA, Hurst GDD, Miller EL, Greig D. 2014. The effect of hybrid transgression on
992 environmental tolerance in experimental yeast crosses. *J. Evol. Biol.* 27:2507–2519.

993 Stenberg S, Li J, Gjuvsland AB, Persson K, Demitz-Helin E, González Peña C, Yue J-X, Gilchrist C, Ärengård
994 T, Ghiaci P, et al. 2022. Genetically controlled mtDNA deletions prevent ROS damage by
995 arresting oxidative phosphorylation.Gruber J, Tyler JK, Toledano MB, editors. *eLife* 11:e76095.

996 Struck TH, Feder JL, Bendiksby M, Birkeland S, Cerca J, Gusarov VI, Kistenich S, Larsson K-H, Liow LH,
997 Nowak MD, et al. 2018. Finding Evolutionary Processes Hidden in Cryptic Species. *Trends in*
998 *Ecology & Evolution* 33:153–163.

999 Tange O. 2011. Gnu parallel-the command-line power tool. *Usenix Mag* 36:42.

1000 Thompson KA, Brandvain Y, Coughlan JM, Delmore KE, Justen H, Linnen CR, Ortiz-Barrientos D,
1001 Rushworth CA, Schneemann H, Schumer M, et al. 2023. The Ecology of Hybrid Incompatibilities.
1002 *Cold Spring Harb Perspect Biol*:a041440.

1003 Tusso S, Nieuwenhuis BPS, Weissensteiner B, Immler S, Wolf JBW. 2021. Experimental evolution of
1004 adaptive divergence under varying degrees of gene flow. *Nat Ecol Evol* 5:338–349.

1005 Villa SM, Altuna JC, Ruff JS, Beach AB, Mulvey LI, Poole EJ, Campbell HE, Johnson KP, Shapiro MD, Bush
1006 SE, et al. 2019. Rapid experimental evolution of reproductive isolation from a single natural
1007 population. *Proceedings of the National Academy of Sciences* 116:13440–13445.

1008 Westram AM, Stankowski S, Surendranadh P, Barton N. 2022. What is reproductive isolation? *Journal of*
1009 *Evolutionary Biology* 35:1143–1164.

1010 Zackrisson M, Hallin J, Ottosson L-G, Dahl P, Fernandez-Parada E, Ländström E, Fernandez-Ricaud L,
1011 Kaferle P, Skyman A, Stenberg S, et al. 2016. Scan-o-matic: High-Resolution Microbial Phenomics
1012 at a Massive Scale. *G3 Genes|Genomes|Genetics* 6:3003–3014.

1013 Zhang Z, Bendixsen DP, Janzen T, Nolte AW, Greig D, Stelkens R. 2020. Recombining Your Way Out of
1014 Trouble: The Genetic Architecture of Hybrid Fitness under Environmental Stress. *Molecular*
1015 *Biology and Evolution* 37:167–182.

1016

1017 **Data Accessibility and Benefit-Sharing Section**

1018 Phenotypic data are available in Table S1. The raw sequences were deposited in the European
1019 Nucleotide Archive, parental populations are available at accession number PRJEB46680, while hybrids
1020 are available at accession number PRJEB83568. The code used for analyses and plotting are available at
1021 https://github.com/devinbendixsen/EvolvingRI. Benefits from this research accrue from the sharing of
1022 our data and results on public databases as described above.

1023

1024 **Author Contributions**

1025 Conceived research: Rike Stelkens; Designed research: Rike Stelkens, Ciaran Gilchrist; Performed
1026 research: Devin P. Bendixsen, Ciaran Gilchrist, Chloé Haberkorn, Karl Persson; Contributed new reagents
1027 or analytical tools: Karl Persson, Jonas Warringer; Data analysis: Devin P. Bendixsen, Chloé Haberkorn,
1028 Karl Persson; Writing: Rike Stelkens, Devin P. Bendixsen, Chloé Haberkorn, Ciaran Gilchrist; Funding
1029 acquisition: Rike Stelkens, Devin P. Bendixsen, Cecilia Geijer, Jonas Warringer.